

Photosensitization versus Photocyclization: Competitive Reactions of Phenylphenalenone in its Role as Phytoanticipins in Plant Defense Strategies

*Josep Casellas, Mar Reguero**

Departament de Química Física i Inorgànica, Universitat Rovira i Virgili, Marcel·lí Domingo,1,
43007-Tarragona. Spain.

ABSTRACT. Phenalenone derivatives are involved in plant defense strategies, producing molecular singlet oxygen in a photosensitization process. Many experimental and theoretical studies determined that phenalenone (PN) can carry out this process with a quantum yield close to one. However, it has been observed that the efficiency of some of its derivatives is much lower. This is the case of 9-phenylphenalenone (9-PhPN). To elucidate the factors that determine the different photochemistry of PN and its derivate 9-PhPN, we have developed a CASSCF/CASPT2 study where several deactivation paths through the lowest excited states have been explored. We have found that the characteristics of the low-lying excited states are similar for both PN and 9-PhPN in the areas near the geometry of excitation. Consequently, the first processes that take place immediately after absorption are possible in both systems, including the population of the triplet state responsible for oxygen sensitization. However, 9-PhPN can also undergo cyclisation by a bond formation between the carbonyl oxygen and a carbon atom of the phenyl substituent. This

process competes favourably with population of triplet states and is responsible for the decrease of the quantum yield of oxygen sensitization in 9-PhPN relative to PN.

INTRODUCTION

Through evolution, plants have developed a variety of strategies to counteract affections of harmful pathogens and adverse environmental conditions. This variety of biological responses is a necessity given the variety of possible harmful agents and the inability of plants to migrate to more favourable locations. One of the most common responses is the synthesis of secondary phytochemical metabolites with antifungal and antimicrobial properties. This route has also been explored for developing novel crop protection strategies and for medical applications. The phytochemicals synthesised by plants can be classified into two groups depending on when they are produced either prior (phytoanticipins) or de novo upon stress (phytoalexins). Due to the broad spectrum of toxicity of these not essential metabolites, its regulation is essential in order to avoid autotoxicity.^{1,2}

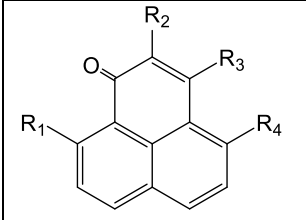
In general, the protective effect of phytoalexins and phytoanticipins involves the intervention of highly reactive singlet oxygen, $^1\text{O}_2$, generated from the oxygen present in the air (basically in its triplet state) by the phytochemical when excited by light. This process is known as photosensitization and operates through the transfer of energy between two species: the initial receptor of light or photosensitizer agent (PS, in this case the phytochemical) and the secondary receptor (R, in this case triplet oxygen), that gives place to the final product (in this case $^1\text{O}_2$). The photosensitization mechanisms can consist of a redox photoreaction (type 1) or in an electronic energy transfer through the excited states (type 2) which is the most common in plant species. However, in order to accomplish successfully this process, several conditions have to be fulfilled:

first, the PS excited state has to be sufficiently long-lived (usually a triplet state). Second, given that this triplet state will not be easily populated by direct absorption, it has to be efficiently populated by deactivation from the state excited by irradiation. On top of these conditions, it is frequent to find a significant overlap between PS emission and R absorption. This is not an indispensable condition, though, given that non-vertical energy transfer is also possible in systems with low-frequency modes involved in the excited-state relaxation process.³ In many cases of photosensitization, both $O_2(^1\Delta_g)$ (the first singlet excited state of molecular oxygen) and $O_2(^1\Sigma_g^+)$ (its second singlet excited state) are formed, given the low energy of both excited states (approximately 23 and 38 kcal·mol⁻¹ respectively), but the $O_2(^1\Sigma_g^+) \rightarrow O_2(^1\Delta_g)$ deactivation is very fast and efficient so finally all the excited oxygen is recovered as $O_2(^1\Delta_g)$.⁴

One of the best examples where this mechanism takes place is in perinaphthenone, also called phenalenone (PN), which is a universal reference for sensitization of singlet oxygen because the quantum yield of this production is close to unity in many solvents.^{5,6,7} In order to contribute to the deep understanding of these compounds, our group studied computationally in a previous work the precise mechanism to populate the sensitizer state of phenalenone. Our findings were in very good agreement with experimental studies, what supports its veracity.⁸ However, not all natural phenalenone derivatives show the same efficiency in the photosensitization process (see Table 1). The reason why the plants synthesize several of these derivatives has been suggested to be the modulation or regulation of singlet oxygen production according to the needs of the plant, avoiding autotoxicity as much as possible. Phenylphenalenones (PhPN), in particular, show extreme behaviours: 3- and 4-phenylphenalenones have large quantum yields of photosensitization, like PN, in contrast with 9-PhPN that present remarkably low values for the same parameter. This differential behaviour has attracted a strong interest, so it can be worth exploring the factors that

modulate their efficiency as singlet oxygen producers. Following this line, the main objective of this study is to explain the special photochemical properties of 9-PhPN.

Table 1. Quantum yields determined experimentally in air-saturated benzene solutions for different phenylphenalenone derivatives in comparison with parent system phenalenone.⁹

	R₁	R₂	R₃	R₄	Φ
	H	H	H	H	0.95
	Ph	H	H	H	0.08
	o-NO ₂ (Ph)	H	H	H	0.51
	H	H	p-MeO(Ph)	H	0.94
	H	MeO	H	Ph	0.72

In the 1970s Cooke detected the presence of 9-PhPN compounds in some plant species.^{10,11} However, the function of these compounds was not clear until Luis and col.¹² and Binks¹³ uncovered a probable relationship between 9-PhPN and phytoanticipin properties. Since then, many other studies have found evidences of this nature in different plants where 9-PhPN is present.^{14,15,16} In order to confirm their protective function, Schneider et al.^{17,18} measured the amount of 9-PhPN in various parts of the plants (roots, leaves, stems...) of different ages and concluded that the roots contained the highest concentration and mostly in younger areas. The same distribution was known to be followed by other compounds of proven phytoalexin properties and, therefore, 9-PhPN was labelled as such.^{19,20}

Its antimicrobial properties were measured by the effect of the compound on an established fungi colony.²¹ The results indicated that this derivative showed slightly reduced activity in comparison with the parent PN although significant compared with other species. Similar results were obtained several years later in an expanded screening of derivatives indicating that unmethylated compounds (like the 9-PhPN studied) are potent antifungals.^{22,23} In the same line, a

strong positive correlation was found between 4-PhPN and 9-PhPN concentrations and the resistance to fungal infections,²⁴ although it was not demonstrated to which extent the individual compounds contributed to the combined effect. This work also suggests that 9-PhPN could be the inactive precursor from which the plant usually avoid the production of singlet oxygen and that would be converted in 4-PhPN only when there is a pressing need of defense. These interconversion reactions were explored in natural conditions and an intricate network of connections was found.²⁵

In order to explain the reduction of the quantum yield of photosensitization in 9-PhN, Nonell *et al.* proposed that it was caused by a photoinduced intramolecular charge-transfer (CT) process from the electron-rich phenyl to the PN moiety.^{9,26} This assumption was supported by evidences on systems where electron transfer in 9-PhPN is inhibited (for example by linking a nitro group to the *ortho* position of the phenyl) that showed a recovery of the quantum yield. Spectroscopic information also suggested that a different state was populated afterwards, the long-life of which indicated that it should have triplet character. However, the first step of the process (excited singlet 9-PhPN, 9-PhPN*, to singlet CT species) was not produced in a single step but it had to involve intermediate species, explained in terms of conformational changes of the phenyl ring. These evidences were used to propose a reaction sequence of photocyclisation in order to produce the remarkably stable radical naphthoxanthenyl.²⁷

In this work, we will focus on the determination of the factors that make decrease the quantum yield of production of photosensitized singlet oxygen by 9-PhPN in comparison with the parent system PN. The working hypothesis is that sensitization competes with another excited state process that can occur in 9-PhPN but neither in PN nor in 4-PhPN, that has been proposed to be the cyclisation reaction depicted in Figure 1. The reaction path of this process has been searched

for in the singlet manifold, because the photosensitization process is linked to triplet states, although both, singlet and triplet excited potential energy surfaces (PESs) have been examined. The work described in this paper, therefore, complements the scope of the previous study on PN developed by our group.

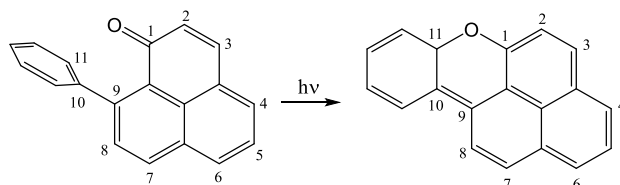


Figure 1. Photocyclisation of 9-PhPN, working hypothesis reaction.

This work has been conducted using the CASSCF methodology and introducing perturbative corrections on the energies through the MS-CASPT2 approach. Using the selected methods, the potential energy surfaces of the ground state and singlet and triplet $n\pi^*$ and $\pi\pi^*$ states have been characterized and minima, crossing points and transition states have been localized. The linear interpolation of internal coordinates has been used in order to properly follow the paths of the reaction between critical points. These results provide accurate information about the competing mechanisms to populate the triplet state manifold versus cyclization along singlet excited states.

COMPUTATIONAL STRATEGY

As already mentioned, this study has been performed using in most of the cases the CASSCF/CASPT2 strategy to describe the PES of the states involved in the reaction. It means that the topography of this surfaces (the location of the critical points, minima and transition states and points of crossing between surfaces) are located at CASSCF level, while the energies of these points are recalculated at the CASPT2 level. But for those states where the dynamic electron

correlation is important, the CASSCF description is not accurate enough (the critical points are not correctly located), and the CASPT2 methodology has been used also to optimize geometries. This method cannot be used in a systematic way due to its high computational cost. An additional factor that increases this cost is the lack of geometrical constraints in the energy calculations. Although the imposition of certain symmetry could be a reasonable approximation to some structures of the system studied here, the reaction coordinates will break it. Consequently symmetry has not been used anywhere, in spite of the additional difficulties that this implies.

The reference wave functions and the molecular orbitals were obtained by state average CASSCF calculations to ensure that all states were orthogonal to each other, which is not necessarily true for state-specific calculations. The interaction of CASSCF states via dynamic correlation is taken into account by the MS-CASPT2 treatment to get an accurate description of the states of interest, which can be analysed through the composition of the Perturbed Modified CAS State Interaction functions (PM-CAS-CI) in terms of the CASSCF wavefunctions. Frequency calculations were also run to determine the nature of the stationary points. Some energy profiles of the PES of interest were obtained following Linear Intrinsic Internal Coordinate paths (LIICs) between critical points of interest.

Numerical gradients were used in the MS-CASPT2 optimizations and frequency calculations due to the lack of implementation of analytical gradients with this protocols. Cholesky decomposition of the two-electron integral matrix has been used.²⁸ In addition, in order to preclude the inclusion of intruder states, an imaginary shift of 0.1 a.u. was included in the zero-order Hamiltonian.²⁹ The CAS state interaction (CASSI) protocol was used to compute the transition oscillator strengths.³⁰

The states analysed in this work were the ground state, the singlet and triplet $n\pi^*$ excited states which are formed by the excitation of one electron of the oxygen lone pair, and the singlet and triplet $\pi\pi^*$ excited states.

All these calculations were performed using the MOLCAS 7.6 package³¹ and a Pople d-polarized split-valence basis set 6-31G (d) except for the conical intersection optimizations where Gaussian 09³² code was used. For the last, state-averaged orbitals were used and the orbital rotation derivative correction to the gradient (which is usually small) was not computed. Full diagonalization method was suppressed in order to make these calculations affordable.

The issue of the chosen active space to be used in the calculations requires a more detailed comment. Given the change in the conjugation of the double bonds between reactant (9-PhPN) and product (naphthoxanthene), the whole π system of the phenalenone moiety and the phenyl substituent should be included in the active space, together with, at least, the n orbital of the oxygen of the carbonyl group. It would mean to have to work with a (22, 21) active space. The need of inclusion of dynamic electron correlation in the description of some states (as will be shown later) and the absence of symmetry in some areas of the PES, make these calculations unfeasible, so a reduction of the size of the active space is compulsory.

To accomplish it, test calculations on the geometry of the ground state minimum of 9-PhPN were performed. These exploratory results showed that in this structure, where the phenyl ring is perpendicular to the molecular plane, the low energy excitations are localized exclusively in the phenalenone moiety. Moreover, the π systems of both moieties did not interact due to their different orientations, so the exclusion of the π system of the phenyl group was an obvious and easy simplification, leaving an active space (16,15) shown in Figure 2. Fortunately, the occupation numbers of some of the orbitals of this space were close to 2 or 0 in all the states of interest, what

indicated that a further reduction to a (12, 11) active space was possible. These 11 orbitals are encircled by the green box in Figure 2. They are 8 delocalized orbitals of the phenalenone π system, the π and π^* orbitals of the carbonyl group and the orbital of the lone pair of the oxygen atom.

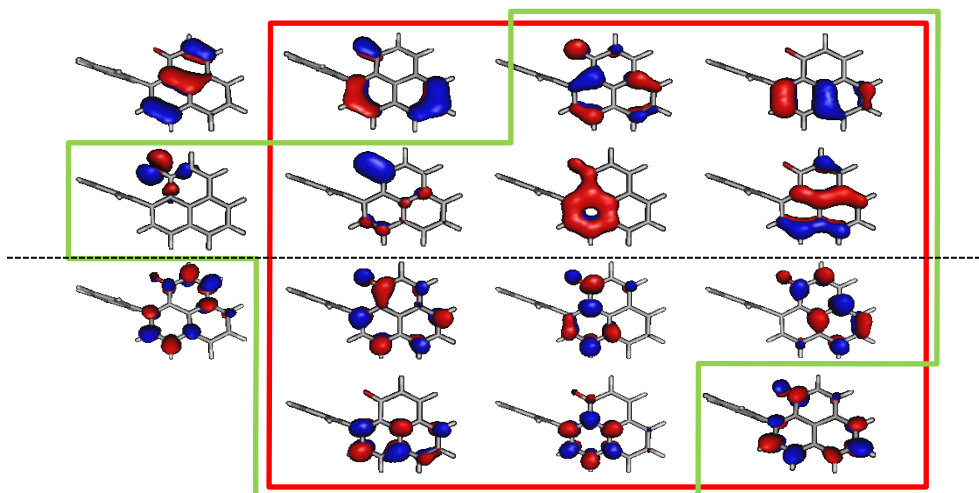


Figure 2. Molecular orbitals of the different active spaces used in the calculations of the Franck Condon (FC) area. Orbitals below the black line are doubly occupied in the ground state, while orbitals above the line are empty. Orbitals in the green box form the (12, 11) active space used to describe S_0 and $^1(n\pi^*)$ states. Orbitals in the red box form the (12, 12) active space used to describe $^1(\pi\pi^*)$ and the $^3(\pi\pi^*)$ states.

However, while this space reproduces accurately the vertical energies of the $^1n\pi^*$ state, the energy of the $^1\pi\pi^*$ state showed a sizable error relative to the experimental value that on the other hand was well reproduced with the (16,15) active space (see Table 2). The alternative to be able to afford the computational cost of this study was to use a different active space to describe the $^1\pi\pi^*$ state, that was finally reduced to (12,12), including the orbitals encircled by the red box in Figure 2, to get the same accuracy in the calculated energies of all the states of interest.

Table 2. MS-CASPT2 energies (in kcal·mol⁻¹) relative to the ground state for the lowest energy states of 9-PhPN at the ground state minimum, obtained with different active spaces.

State	CAS(16,15) ^a	CAS(12,11) ^b	CAS(12,12) ^c	Exp. ^{9,d}
³ ($\pi\pi^*$)	-	66.1	65.1	-
¹ ($n\pi^*$)	72.9	74.4	-	70.3
¹ ($\pi\pi^*$)	84.1	90.8	82.4	80.5
³ ($n\pi^*$)	-	71.7	-	-

^a) Molecular orbitals shown in Figure 2 ^b) Molecular orbitals shown in the red box of Figure 2

^c) Molecular orbitals shown in the green box of Figure 2. ^d) Experimental data from the spectrum of 9-PhPN in benzene solution.

Unfortunately, this is not the only problem aroused by the reduction of the active space. For the cyclised photoproduct, the set of molecular orbitals needed to properly describe the lower energy states is different from the active space used for the reactant. In the photoproduct, there is only a π system that extends to the whole skeleton of the molecule, what includes the phenyl group of the reactant. On top of this, to study the reaction of interest, the new π bond formed must be also included in the active space. To form it, the hybridization of the O and C atoms change from reactant to product so, to properly study this process, the active space should be increased even beyond the initial (22,21) size proposed. Facing the unfeasibility of these calculation, we chose the option of using an active space for the product (and for the transition state of the thermal reaction) equivalent to the (12,11) and (12,12) ones used for the reactant, obtained by the progressive change of the orbitals when doing successive calculations following the path that connects reactant and product. Figure 3 show the shape of the active orbitals at the product geometry. The use of different active spaces implies that the relative energies of the product and

the structures of the zone of the transition state, must be considered only as an approximation to provide a qualitative description of these areas of the PESs of 9-PhPN.

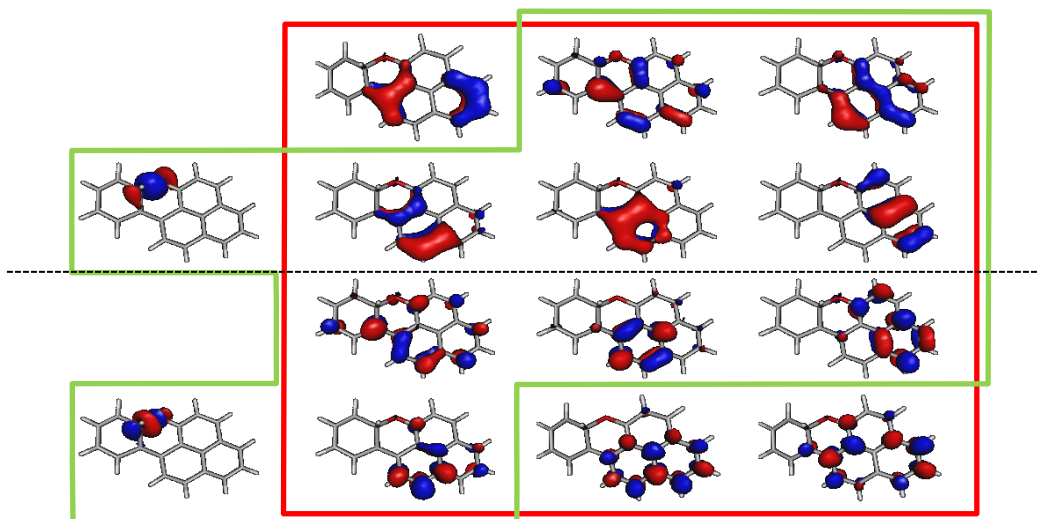


Figure 3. Molecular orbitals of the active space used in the calculations of the photoproduct. Orbitals below the black line are doubly occupied in the ground state, while orbitals above the line are empty. Orbitals in the green box form the (12,11) active space used to describe S_0 and $^1(n\pi^*)$ states. Orbitals in the red box form the (12,12) active space used to describe $^1(\pi\pi^*)$ and the $^3(\pi\pi^*)$ states.

RESULTS AND DISCUSSION

Ground state minima and vertical excitations

The absorption of a photon initiates the reactivity of the studied system from the geometry of minimum energy of the ground state of the 9-PhPN. The optimized geometry, depicted in Figure 4, shows the phenyl substituent almost perpendicular to the planar phenalenone with a dihedral angle of 92.1° . Other relevant parameters are also shown in Figure 4 and relative energies of the lowest singlet and triplet excited states are shown in Table 3 together with oscillator strengths.

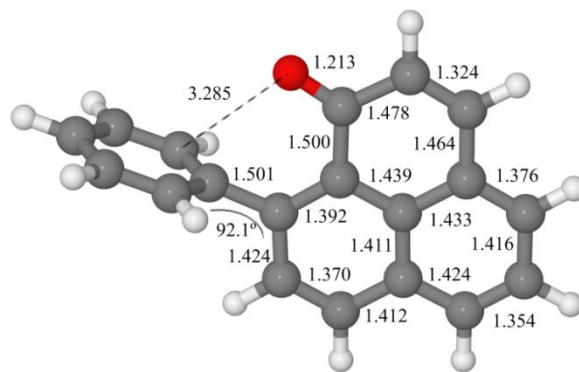


Figure 4. Ground state minimum energy geometry obtained at CASSCF level. Bond distances in angstroms, dihedral angle in degrees

Table 3. Energies (in kcal·mol⁻¹) relative to the ground state, oscillator strengths (f) and dipole moments (μ , in D) for the lowest energy states of 9-PhPN computed at several levels, at the ground state minimum.

State	CASSCF	SS-CASPT2	MS-CASPT2	f	μ
GS	0.0	0.0	0.0	-	3.05
³ ($\pi\pi^*$)	61.1	65.8	65.1	$0.10 \cdot 10^{-3}$	2.99
³ ($n\pi^*$)	74.2	70.1	71.7	$0.26 \cdot 10^{-5}$	0.30
¹ ($n\pi^*$)	77.2	73.0	74.4	$0.47 \cdot 10^{-3}$	0.29
¹ ($\pi\pi^*$)	119.4	108.0	82.4	0.21	3.33

The analysis of the wavefunction of the first singlet excited state indicates that it is described by an excitation of an electron of the lone pair of the oxygen atom to a delocalized π anti-bonding orbital of the phenalenone moiety. This $n\pi^*$ state is located 74.4 kcal·mol⁻¹ above the ground state and its dipole moment is smaller than that of the ground state as a result of the exocyclic charge transfer. The composition of the PM-CAS-CI function shows that the ¹($n\pi^*$) CASSCF state do not interact with any other state, as expected by the orbital symmetry of the oxygen lone pair. For this reason, the multi-state perturbative treatment does not introduce a noticeable change in energy

from the State Specific SS-CASPT2 result. The small value of the oscillator strength indicates a very low probability of transition from the ground state, so this result predicts that this band will not appear in the absorption spectrum of 9-PhPN, in agreement with experimental observations.⁹

The second singlet excited state has a $\pi\pi^*$ character and it is described by an excitation from a delocalized π bonding orbital on the phenalenone moiety to an antibonding orbital. Its oscillator strength is large what indicates that the probability of transition from the ground state is high, so our results predict that this state will absorb the incident radiation. In energetic terms, the $^1(\pi\pi^*)$ state is located $82.4 \text{ kcal}\cdot\text{mol}^{-1}$ above the ground state, which is comparable with the experimental measurements of the maximum absorption wavelength in benzene that locate the state at $80.5 \text{ kcal}\cdot\text{mol}^{-1}$.⁹ The dipole moment of this state is similar to the ground state one, as expected for an excitation of $\pi\pi^*$ character. The large difference between the CASSCF and CASPT2 values indicates that the dynamic electron correlation affects strongly the electronic configuration of this state, which is not properly described at CASSCF level. Consequently, the optimization of critical points cannot be reliably performed by the CASSCF procedure. The MS-CASPT2 results also differ noticeably from the SS-CASPT2 one, because the interaction between CASSCF states due to the electron correlation is important. In fact, the S_2 MS-CASPT2 state shows a strong mixing between the S_3 and S_4 CASSCF states with coefficients 0.63 and 0.64 respectively, both of them of $\pi\pi^*$ character.

The first triplet excited state has $\pi\pi^*$ character and it is the lowest-energy excited state, located $66.0 \text{ kcal}\cdot\text{mol}^{-1}$ above the ground state. Its description is similar to that of the absorbing state. On the other hand, its PM-CAS-CI function does not show mixing of CASSCF states, so it is expected that the description of this state, and consequently the geometry optimization, will be accurate

enough at CASSCF level. The calculated dipole moment is 2.99 Debye, only slightly smaller than that of the singlet state of the same character. The second triplet state has $n\pi^*$ character, similar to the one of the lowest singlet excited state. Its energy is similar to that of the singlet state of the same character and, like in that case, its PM-CAS-CI wavefunction does not show any mixing of states.

The geometry of the proposed photoproduct, naphthoxanthene was also optimized. The geometry obtained is depicted in Figure 5, where some geometrical parameters are also shown. The energies of the lowest states of naphthoxanthene are collected in Table 4. This species is $19.7 \text{ kcal}\cdot\text{mol}^{-1}$ less stable than 9-PhPN, so it is not thermodynamically favoured. To predict if it will be long-lived, it is necessary to calculate the energy barrier of the back reaction to phenalenone. If it is low, this photoproduct will be considered an intermediate in the photochemistry of phenalenone, and consequently a species difficult to be observed.

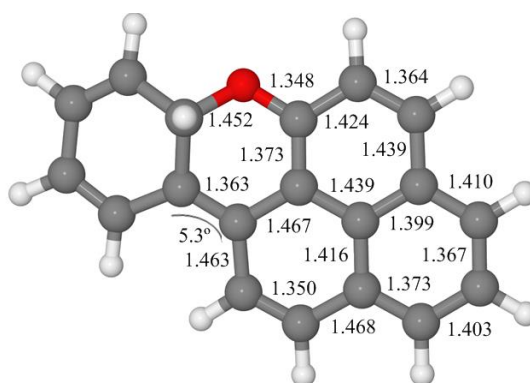


Figure 5. Ground state minimum energy geometry of the product obtained at CASSCF level.

Bond distances in angstroms, dihedral angle in degrees.

Table 4. Energies (in $\text{kcal}\cdot\text{mol}^{-1}$) relative to the ground state, oscillator strengths (f) and dipole moments (μ , in D) for the lowest energy states of naphthoxanthene at the ground state minimum.

In terms of energy (see Table 5), the $^1(n\pi^*)$ minimum is located $58.5 \text{ kcal}\cdot\text{mol}^{-1}$ above the ground state global minimum. It means a relaxation from the Franck Condon zone of $15.9 \text{ kcal}\cdot\text{mol}^{-1}$, and a vertical energy gap with the ground state of $44.4 \text{ kcal}\cdot\text{mol}^{-1}$. The small value of the oscillator strength predicts a very low probability of emission from this species, what rules out the probability of emission from the $^1(n\pi^*)$ state. An exploratory search at CASPT2 level on this PES confirmed the character of a minimum of this structure, indicating that the description of this surface provided by CASSCF is reliable. Table 5 shows that at this geometry singlet $n\pi^*$ and triplet $\pi\pi^*$ states are in close proximity. Due to the character of these states, it is expected that the spin-orbit coupling between them will be large. In this case, if the $^1(n\pi^*)$ minimum is populated, the transfer between the two states through ISC will be very probable, like in the parent compound phenalenone.

Table 5. MS-CASPT2 energies (in $\text{kcal}\cdot\text{mol}^{-1}$) relative to the ground state minimum, dipole moment, μ , in D and oscillator strengths, f , of the lower states of 9-PhPN at the minimum energy geometry of the $^1(n\pi^*)$ state optimized at CASSCF level.

State	MS-CASPT2	μ	f
GS	14.1	3.20	-
$^3(\pi\pi^*)$	56.3	2.60	$0.17\cdot 10^{-2}$
$^1(n\pi^*)$	58.5	0.98	$<10^{-6}$
$^3(n\pi^*)$	58.8	0.97	$<10^{-7}$
$^1(\pi\pi^*)$	76.9	2.63	0.22

$^1(\pi\pi^*)$ state

It can be observed in the PM-CAS-CI wavefunction that there is a strong interaction of the 3rd and 4th CASSCF states, what means that none of those CASSCF wavefunction will describe properly the $^1(\pi\pi^*)$ state, but both will give a rough approximation to it. For this reason, the optimization of this state had to be performed at CASPT2 level. Figure 7 shows the minimum

energy geometries obtained for optimization of the 3rd and 4th roots at CASSCF level and 3rd root at CASPT2 level. It can be observed that, while the distances in the phenalenone moiety are similar in all structures, the dihedral angle of the phenyl ring relative to phenalenone is drastically different, being close to perpendicular at CASSCF level but almost coplanar at CASPT2 level. This geometrical parameter is crucial in the photoreaction of interest. Given that the O-C₁₁ bond must be formed, it is necessary that these atoms get close together, as happens only in the CASPT2 minimum. These results show again that a correct description of the PES that includes the dynamic electron correlation is necessary to correctly determine reaction mechanisms.

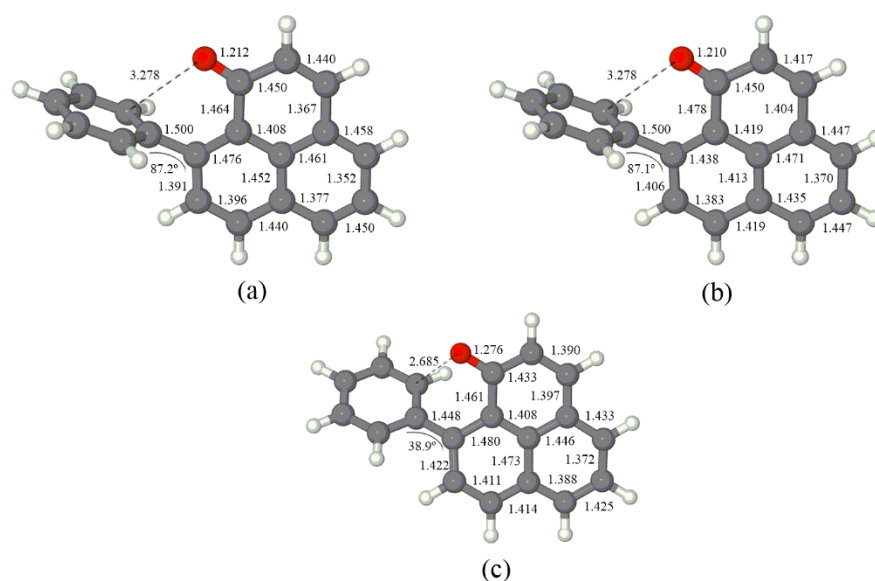


Figure 7. Minimum energy geometries of the $^1(\pi\pi^*)$ state of 9-PhPN obtained as a) 3rd root at CASSCF level b) 4th root at CASSCF level and c) 3rd root at MS-CASPT2 level

Energies (calculated at MS-CASPT2 level) of the CASSCF and CASPT2 minima are collected in Table 6. The energy of the minimum optimized at CASPT2 level is much lower than the energy of the CASSCF minima, what confirms the better performance of the CASPT2 optimization, as it

was expected. This structure is 24.1 kcal·mol⁻¹ more stable than the FC energy of this state, and it is almost isoenergetic with the ¹(nπ*) minimum. Moreover, at all three minima the ¹(ππ*) state is clearly below the ¹(nπ*) and, therefore, it becomes the lowest singlet excited state. These results together with non-negligible values for the oscillator strengths indicate that emission is possible from these species although improbable if the population do not remain enough time in those minima (short-lived species), which depends on the possible paths of depopulation of the ¹(ππ*) minimum that we will analyse further down. The inversion of the S₁ and S₂ states indicates that there must be a conical intersection between these states and that the CI hyperspace must extend for a large range of values of the phenyl dihedral angle.

Table 6. MS-CASPT2 energies (in kcal·mol⁻¹) relative to the ground state minimum, and oscillator strengths, *f*, of the lower states of 9-PhPN at the minimum energy geometries optimized at CASCSF and CASPT2 level for different roots of ππ* state.

<i>State</i>	3 rd CASSCF root		4 th CASSCF root		3 rd CASPT2 root	
	<i>MS-CASPT2</i>	<i>f</i>	<i>MS-CASPT2</i>	<i>f</i>	<i>MS-CASPT2</i>	<i>f</i>
GS	15.0	-	7.6	-	6.9	-
³ (ππ*)	56.5	0.58·10	53.9	0.43·10	49.0	0.26·10 ⁻³
³ (nπ*)	74.3	< 10 ⁻⁵	70.7	< 10 ⁻⁷	62.2	< 10 ⁻⁴
¹ (nπ*)	74.9	< 10 ⁻⁵	72.5	0.20·10	64.8	0.05
¹ (ππ*)	71.0	0.17	68.9	0.19	58.3	0.13

³(ππ*) and ³(nπ*) states

The minimum energy structures of these states were also located at CASSCF level and they are shown in Figure 8. As can be seen in this figure, both geometries have the phenyl perpendicular to the molecular plane but present very different CO distances, which is also the main difference between the CASSCF singlet state minima.

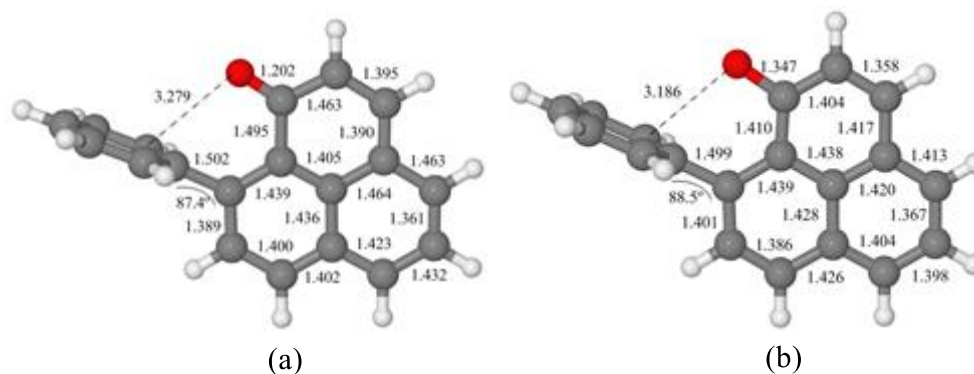


Figure 8. Minimum energy geometries of the a) $^3(\pi\pi^*)$ state and b) $^3(n\pi^*)$ of 9-PhPN obtained optimizing at CASSCF level.

The vertical energies are exposed in Table 7 for both structures. In spite that the composition of the PM-CAS-CI of the $^3(\pi\pi^*)$ state does not show a mixing of CASSCF states and, therefore, we could assume that CASSCF level describes properly this state, the minimum located at this level does not seem to be, in fact, the minimum energy point on the $^3(\pi\pi^*)$ surface.

Table 7. MS-CASPT2 energies (in kcal·mol⁻¹) relative to the ground state minimum of the lowest excited states at the $^3(\pi\pi^*)$ and $^3(n\pi^*)$ minima optimized at CASSCF level.

State	$^3(\pi\pi^*)$ state		$^3(n\pi^*)$ state	
	MS-CASPT2	<i>f</i>	MS-CASPT2	<i>f</i>
GS	8.1	-	10.1	-
$^3(\pi\pi^*)$	51.0	<10 ⁻⁶	54.3	<10 ⁻⁵
$^3(n\pi^*)$	71.6	<10 ⁻⁷	57.0	<10 ⁻⁷
$^1(n\pi^*)$	73.4	<10 ⁻⁵	58.9	<10 ⁻⁶
$^1(\pi\pi^*)$	72.1	0.28	77.4	0.25

Having a look at the energies of this state at the geometries of the $^1(\pi\pi^*)$ minima in

Table 6, we observed that the energy of the $^3(\pi\pi^*)$ is lower in the geometry where the phenyl group has a dihedral angle of 38.9°, far from the 87.4° predicted at CASSCF level. Given that the

exact location of the minimum of this state will not be of crucial interest and the cost of the CASPT2 optimization is high, we will assume that the geometry of the $^3(\pi\pi^*)$ minimum will be similar to that of the $^1(\pi\pi^*)$ one. What is important is that the $^3(\pi\pi^*)$ minimum is the most stable one, being around $10 \text{ kcal}\cdot\text{mol}^{-1}$ more stable than those of the singlet excited species. On the other hand, the relative energy of the $^3(n\pi^*)$ state is only slightly lower in its minimum than in the $^1(n\pi^*)$ minimum, which indicates again that the PES of these states must be similar.

Reaction mechanisms

Thermal isomerization path along the ground state

The transition state of the path connecting the reactant (9-PhPN) and the cyclized product was searched for. The geometry obtained (see Figure 9) shows a substantial deviation of the phenyl ring from planarity (dihedral angle: 30°). The C₉-C₁₀, C₁-O and C₁₁-O bond distances are intermediate between the reactant's and product's values. Due to the formation of the C₁₁-O bond, C₁₁ becomes sp³ and acquires a tetrahedral structure.

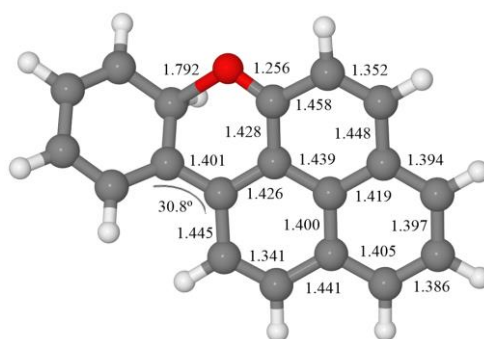


Figure 9. Transition state geometry on the ground state obtained at CASSCF level and confirmed at MS-CASPT2 level.

This TS is 25.6 kcal·mol⁻¹ above the 9-PhPN minimum, and 4.8 kcal·mol⁻¹ higher in energy than the product. It means that the process is easily reversible from there, so the product will be very short-lived. Nevertheless, it must be pointed out that these energies should be taken only as qualitative data, given that the active spaces used to calculate them are not equivalent. To get a value of the energy barrier quantitatively precise, the energies of reactant, product and transition state should be calculated with a larger active space, which should include also the π system of the phenyl ring, given that these molecular orbitals are also modified along the reaction. Such CASPT2 calculations are not feasible as routine work.

Photochemical reaction paths

The only state that shows a certain probability of absorbing the initial irradiation in 9-PhPN is the ¹($\pi\pi^*$) state. We can assume then that the photochemical process starts at the Franck Condon geometry of the PES of this state, located 82.4 kcal·mol⁻¹ above the ground state minimum. The aforementioned assumption is also validated through the analysis of the available experimental spectra, which indicates that there is no other band present.⁹ From the theoretical point of view, the probability of absorption of the initial excitation by the ¹($n\pi^*$) is very low. It could increase if orbital symmetry restrictions were broken by the loss of planarity of the phenalenone moiety by vibrational movements, but this is not probable due to the rigidity of this fragment given by the conjugation of its π system.

Once on the ¹($\pi\pi^*$) state, the energy of the ¹($n\pi^*$) is not close enough to predict an internal conversion between them, so the most probable initial process will be relaxation along the ¹($\pi\pi^*$) PES. In principle this relaxation would lead to the ¹($\pi\pi^*$) minimum where the bond distances of the phenalenone moiety are slightly changed and the phenyl ring has rotated approximately 60°.

But, although this downhill path is the most favoured thermodynamically because leads to the lowest energy structure, the rotation of the phenyl ring is a drastic geometrical change that can be hindered by the solvent and, in any case, will be slower than the change of bond distances. We cannot discard, then, the population of areas of the $^1(\pi\pi^*)$ PES of geometries similar to the structure given by the CASSCF optimization of this state (where the phenyl ring has hardly rotated).

Given that the $^1(\pi\pi^*)$ and $^1(n\pi^*)$ states are inverted at both geometries (CASSCF and CASPT2 minima) relative to the energetic ordering at FC, these surfaces must cross along the paths that lead from FC to those geometries. Exploring the S_1 and S_2 surfaces by means of LIICs, crossing points along both paths were located. It would be desirable to find the lowest energy point of these crossings, but this calculation would not give reliable results, given that this optimization can only be performed at CASSCF level, where the $^1(\pi\pi^*)$ state is very poorly described. The structures of the crossings shown in Figure 10, then, are not optimized, so the energies of these points of degeneracy give upper limits of the barriers of internal conversion between the $^1(\pi\pi^*)$ and $^1(n\pi^*)$ states.

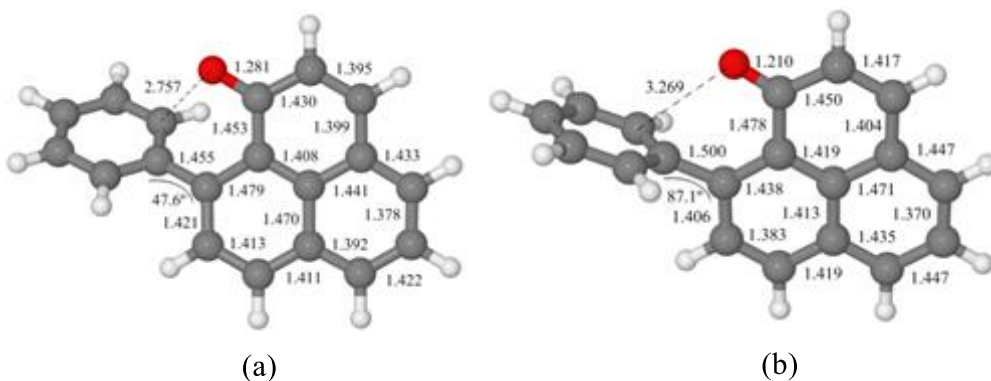


Figure 10. Points of the ${}^1\pi\pi^*/{}^1n\pi^*$ conical intersection hyperspace. Geometries obtained in the LIICs from FC to (a) the CASPT2 minimum (*rot*-CI) (b) the CASSCF minimum (*perp*-CI).

The structure shown in Figure 10 (b), where the phenyl ring is almost perpendicular to the phenalenone moiety (*perp*-CI), is found to be $70.1 \text{ kcal}\cdot\text{mol}^{-1}$ above the ground state global minimum, while the structure shown in Figure 10 (a) (*rot*-CI) is only $62.4 \text{ kcal}\cdot\text{mol}^{-1}$ high. To check if both crossing points are accessible in the relaxation route from FC, the profiles of the lowest energy surfaces along the LIICs from FC to these geometries were calculated. The results (shown in Figure S1 of SI) show that these points are accessible from the FC region along barrierless paths. Crossing to the ${}^1(n\pi^*)$ surface can then take place also easily since on this surface the system will continue relaxing towards the minimum energy point of this state. It should be noted that ${}^1(n\pi^*)$ and ${}^1(\pi\pi^*)$ minima are almost isoenergetic ($58.5 \text{ kcal}\cdot\text{mol}^{-1}$ and $58.3 \text{ kcal}\cdot\text{mol}^{-1}$ respectively) and they are connected through the *rot*-CI that, as explained before, provides an upper limit for the barrier of this interconversion, that is only around $4.0 \text{ kcal}\cdot\text{mol}^{-1}$ from any of the minima. It means that, independently of the relaxation path followed from FC, and independently of which minimum will be initially populated from the *perpendicular* or *rotated* conical intersections, the ${}^1n\pi^*$ and ${}^1\pi\pi^*$ species are directly connected so an equilibrium is expected to be established between the population of both minima. The subsequent relaxation process can then take place from any of them.

From these points, three probable processes open up. First, radiative deactivation (fluorescence) from the ${}^1(\pi\pi^*)$ minimum since the oscillator strength to the ground state has a non-negligible value. The lifetime depends on the other possible channels of depopulation of this minimum, which are analysed in the following points.

Second, an intersystem crossing from the $^1(n\pi^*)$ minimum to the $^3(\pi\pi^*)$ state can take place since their energies are quasi-degenerated and the spin-orbit coupling between them is predicted to be large. However, if the system reaches the $^3(\pi\pi^*)$ state minimum, the energy transfer to the triplet oxygen becomes possible, giving place to oxygen sensitization.

Finally, an internal conversion to the ground state is also possible. A conical intersection between the $^1(n\pi^*)$ and ground state was located at CASSCF level (and confirmed at CASPT2 level) at the geometry shown in Figure 11. At this structure, the dihedral angle of the phenyl ring is still 37° , far from planarity, but the carbonyl double bond can be considered almost broken, while the new σ bond is not completely formed. This CI is located $54.8 \text{ kcal}\cdot\text{mol}^{-1}$ above the ground state minimum, and lower in energy than both $^1(n\pi^*)$ and $^1(\pi\pi^*)$ state minima.

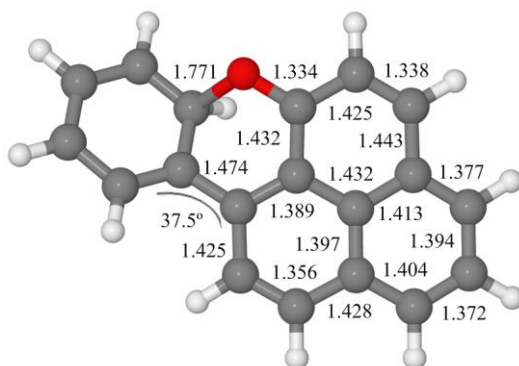


Figure 11. Minimum energy geometry of the S_1/S_0 conical intersection optimized at CASSCF level and confirmed at MS-CASPT2 level.

Following this last process, the analysis of the correlation between the states of reactant and product at the valence-bond level, indicates that the ground state of the product correlates with the $^1(n\pi^*)$ state of the reactant. The n orbital of the oxygen is oriented towards the p orbital of the C_{11} of the phenyl group, which are close together at the geometry of the optimized CI. In the $^1(n\pi^*)$

state, the n orbital is mono-occupied, what allows the formation of a σ bond with the p orbital of C₁₁. This cyclisation is possible in 9-PhPN, but not in PN or in 4-PhPN.

To confirm that this conical intersection is accessible, the profiles of the lowest energy surfaces along the LIIC from the $^1n\pi^*/^1\pi\pi^*$ CIs to the S₁/S₀ CI were calculated (Figure S3 of SI). In terms of energy, an energy barrier of 10.0 kcal·mol⁻¹ is found from the *rot*-CI while it is only of 3.5 kcal·mol⁻¹ from the *perp*-CI, due to the higher energy of this latter CI. These are in fact upper bounds for the energy of the real barrier, and anyway the system will have enough residual kinetic energy from the initial excitation (82.4 kcal·mol⁻¹) to surmount these small local barriers and reach the S₁/S₀ CI.

Finally, the relaxation from the conical intersection to the product on the ground state surface has also been analysed, to confirm that this relaxation path is possible, by means of a LIIC path calculated from the S₁/S₀ CI to the photoproduct (Figure S4 of SI). The results indicate that the final C₁₁-O bond formation follows a barrierless path to the product ground state. At the same time, the S₁ surface increases its relative energy. The reaction cycle would finish with the return via a thermal path to 9-PhPN along the ground state.

Global description of the proposed mechanism

The global landscape that these results describe is shown in Figure 12.

the $^1(n\pi^*)$ and $^3(\pi\pi^*)$ states will be large, according to Kasha's rules and similarly to what was found for phenalenone in the previous work of the group on this system.⁸

The last possible process is an internal conversion from the $^1(n\pi^*)$ state to the ground state through a conical intersection located between these surfaces. To reach this crossing point, a small barrier of less than $4 \text{ kcal}\cdot\text{mol}^{-1}$ must be overcome, but the energy absorbed in the initial excitation is enough to surmount it. Once on the ground state, the system can return to the initial reactant or to the cyclised photoproduct, which will finally revert to the original 9-PhPN through a thermal reaction along the ground state surface.

This last step seems to be the most favoured thermodynamically and kinetically, because it leads to the most stable minimum and competes favourably with the alternative slow processes of ISC and radiative decay. Nevertheless, none of these last phenomena is discarded to happen, so the population of the $^3(\pi\pi^*)$ minima and emission from the $^1(\pi\pi^*)$ species can also happen to a certain extent. The small population of the triplet manifold would explain the low quantum yield of 9-PhPN for singlet oxygen production.

To predict computationally the preferential reaction paths and the quantum yields of the different possible phenomena, it would be necessary to perform dynamic calculations, where kinetic factors are considered together with the thermodynamic factors given by the topography of the potential energy surfaces described here. Such study, though, is beyond the scope of this work.

CONCLUSIONS

The photochemistry of 9-phenylphenalenone has been studied to understand why the oxygen sensitization efficiency of this compound is much smaller than the one of its parent compound, phenalenone. This study has been performed by means of ab initio calculations, using the CASSCF

and CASPT2 methods. Due to the complexity of the reactivity and the large size of the system, reductions in the most adequate active space have had to be performed.

We have found that both PN and 9-PhPN have similar topography and energies of the $^1(n\pi^*)$, $^1(\pi\pi^*)$, $^3(\pi\pi^*)$ and $^3(n\pi^*)$ surfaces in the areas near the Frank Condon geometry. Consequently, the processes that take place in these zones, i. e. emission from the $^1(\pi\pi^*)$ species and oxygen sensitization from the $^3(\pi\pi^*)$ minimum, will be possible in both systems. But 9-PhPN also has an alternative reaction path, which is cyclisation by a bond formation between the carbonyl oxygen and a carbon atom of the phenyl substituent. This process is predicted to be more efficient than the previous ones, decreasing consequently the quantum yield of oxygen sensitization. On the other hand, luminescence from the $^1(\pi\pi^*)$ species is expected to be more probable since this state becomes the first excited one in its minimum, unlike in phenalenone where this behaviour is not observed. This emission agrees with the weak fluorescence experimentally observed.⁹

As a whole, the difference of quantum yield of oxygen sensitization observed experimentally between PN and its derivative 9-PhPN has been explained satisfactorily. The results obtained agree satisfactorily with the experimental data and observations. The approximations applied in the computational methods seem to have been appropriate.

ASSOCIATED CONTENT

Supporting Information. Figure S1: MS-CASPT2 profiles of the PES of the lowest singlet energy states of 9-PhPN along the LIIC from the FC geometry to the $^1\pi\pi^*/^1n\pi^*$ crossings, perp-CI and rot-CI. Figure S2: MS-CASPT2 profiles of the PES of the lowest energy states of 9-PhPN along the LIIC from the minimum energy point of the $n\pi^*$ state to the $^1\pi\pi^*/^1n\pi^*$ crossings, perp-CI and rot-CI. Figure S3: LIIC profiles of the PES of the lowest energy states from the $^1\pi\pi^*/^1n\pi^*$ rot-CI

to the S_1/S_0 conical intersection. Figure S4: LIIC profiles of the PES of the lowest energy states from the minimum energy point of the S_1/S_0 CI to the minimum energy geometry of the cyclized product.

AUTHOR INFORMATION

Corresponding Author

*E-mail: mar.reguero@urv.cat

Author Contributions

M. R. conceived and designed the study; J. C. performed the calculations. The manuscript was written through contributions of all authors. All authors have given approval to the final version of the manuscript.

Funding Sources

Financial support has been provided by the Spanish Administration (Project CTQ2014-51938-P), the Generalitat de Catalunya (Projects 2014SGR199 and Xarxa d'R+D+I en Química Teòrica i Computacional, XRQTC) and the European Union (COST Action ECOST-Bio CM1305).

ACKNOWLEDGMENT

We want to thank the Spanish Administration, the Generalitat de Catalunya and the European Union for their financial support.

REFERENCES

1. Paxton, J. A new working definition of the term, phytoalexin. *Plant Dis.* **1980**, *64*, 734-734.
2. VanEtten, H. D.; Mansfield, J. W.; Bailey, J. A.; Farmer, E. E. Two classes of plant antibiotics: phytoalexins versus "phytoanticipins". *Plant Cell* **1994**, *6*, 1191-1992.

3. Frutos, L. M.; Castaño, O.; Andrés, J. L.; Merchán, M.; Acuña, A. U. A theory of nonvertical triplet energy transfer in terms of accurate potential energy surfaces: The transfer reaction from π, π^* triplet donors to 1,3,5,7-cyclooctatetraene. *J Chem Phys.* **2004**, *120*, 1208-1216.
4. Schweitzer, C.; Schmidt, R. Physical mechanisms of generation and deactivation of singlet oxygen. *Chem. Rev.* **2003**, *103*, 1685-1757.
5. Schmidt, R.; Tanielian, C.; Dunsbach, R.; Wolff, C. Phenalenone, a universal reference compound for the determination of quantum yields of singlet oxygen $O_2(^1\Delta_g)$ sensitization. *J. Photochem. Photobiol. A* **1994**, *79*, 11-17.
6. Martí, C.; Jürgens, O.; Cuenca, O.; Casals, M.; Nonell, S. Aromatic ketones as standards for singlet molecular oxygen $O_2(^1\Delta_g)$ photosensitization. Time-resolved photoacoustic and near-IR emission studies. *J. Photochem. Photobiol. A* **1996**, *97*, 11-18.
7. Oliveros, E.; Bossmann, S. H.; Nonell, S.; Martí, C.; Heit, G.; Tröscher, G.; Neuner, A.; Martínez, C.; Braun, A. M. Photochemistry of the singlet oxygen [$O_2(^1\delta(g))$] sensitizer perinaphthenone (phenalenone) in N,N'-dimethylacetamide and 1,4-dioxane. *New J. Chem.* **1999**, *23*, 85-93.
8. Segado, M.; Reguero, M. Mechanism of the photochemical process of singlet oxygen production by phenalenone. *Phys. Chem. Chem. Phys.* **2011**, *13*, 4138-4148.
9. Flors, C.; Ogilby, R.; Luis, J. G.; Grillo, T. A.; Izquierdo, L. R.; Gentili, P-L.; Bussoti, L.; Nonell, S. Phototoxic phytoalexins. Processes that compete with the photosensitized production of singlet oxygen by 9-phenylphenalenones. *Photochem. Photobiol.* **2006**, *82*, 95-103.

10. Cooke, R. G.; Thomas, R. L. Colouring matters of australian plants. XX: Synthesis of hydroxyanigorufone and related phenalenones. *Aust. J. Chem.* **1975**, *28*, 1053-1057.
11. Cooke, R. G.; Dagley, I. J. Colouring matters of australian plants. XVIII: Constituents of anigozanthos rufus. *Aust. J. Chem.* **1978**, *31*, 193-197.
12. Luis, J. G.; Fletcher, W. Q.; Echeverri, F.; Grillo, T. A.; Perales, A.; González, J. A. Intermediates with biosynthetic implications in de novo production of phenyl-phenalenone-type phytoalexins by *Musa acuminata* revised structure of emenolone. *Tetrahedron* **1995**, *51*, 4117-4130.
13. Luis, L. G.; Quiñones, W.; Echeverri, F.; Grillo, T. A.; Kishi, M. P.; Garcia-Garcia, F.; Torres, F.; Cardona, G. Musanolones: Four 9-phenylphenalenones from rhizomes of *Musa acuminata*. *Phytochem.* **1996**, *41*, 753-757
14. Luis, J. G.; Lahlou, E. H.; Andrés, L. S.; Echeverri, F.; Fletcher, W. Q. Phenylphenalenonic phytoanticipins. New acenaphthylene and dimeric phenylphenalenones from the resistant *Musa* selected hybrid SH-3481, *Tetrahedron* **1997**, *53*, 8249-8256.
15. Kamo, T.; Kat, N.; Hirai, N.; Tsuda, M.; Fujioka, D.; Ohigashi, H. Phenylphenalenone-type phytoalexins from unripe buñgulan banana fruit. *Biosci. Biotechnol. Biochem.* **1998**, *62*, 95-101.
16. Kamo, T.; Hirai, N.; Iwami, K.; Fujioka, D.; Ohigashi, H. New phenylphenalenones from banana fruit. *Tetrahedron* **2001**, *57*, 7649-7675.
17. Opitz, S.; Schneider, B. Organ-specific analysis of phenylphenalenone-related compounds in *Xiphidium caeruleum*. *Phytochemistry* **2002**, *61*, 819-825.

18. Schneider, B.; Paetz, C.; Hölscher, D.; Opitz, S. HPLC-NMR for tissue-specific analysis of phenylphenalenone-related compounds in *Xiphidium caeruleum* (Haemodoraceae). *Magn. Reson. Chem.* **2005**, *43*, 724-728.
19. Lazzaro, A.; Corominas, M.; Martí, C.; Flors, C.; Izquierdo, L. R.; Grillo, T. A.; Luis, J. G.; Nonell, S. Light- and singlet oxygen-mediated antifungal activity of phenylphenalenone phytoalexins. *Photochem. Photobiol. Sci.* **2004**, *3*, 706-710.
20. Echeverri, F.; Torres, F.; Quiñones, W.; Escobar, G.; Archbold, R. Phenylphenalenone phytoalexins, will they be a new type of fungicide? *Phytochem. Rev.* **2012**, *11*, 1-12.
21. Quiñones, W.; Escobar, G.; Echeverri, F.; Torres, F.; Rosero, Y.; Arango, V.; Cardona, G.; Gallego, A. Synthesis and antifungal activity of *Musa* phytoalexins and structural analogs *Molecules* **2000**, *5*, 974-980.
22. Otálvaro, F.; Nanclares, J.; Vásquez, L. E.; Quiñones, W.; Echeverri, F.; Arango, R.; Schneider, B. Phenalenone-type compounds from *Musa acuminata* var. "Yangambi km 5" (AAA) and their activity against *Mycosphaerella fijiensis*. *J. Nat. Prod.* **2007**, *70*, 887-890.
23. Otálvaro, F.; Jitsaeng, K.; Munde, T.; Echeverri, F.; Quiñones, W.; Schneider, B. O-Methylation of phenylphenalenone phytoalexins in *Musa acuminata* and *Wachendorfia thyrsoiflora*. *Phytochemistry* **2010**, *71*, 206-213.
24. Otálvaro, F.; Echeverri, F.; Quiñones, W.; Torres, F.; Schneider, B. Correlation between phenylphenalenone phytoalexins and phytopathological properties in *Musa* and the role of a dihydrophenylphenalene triol. *Molecules* **2002**, *7*, 331-340.

25. Opitz, S.; Hölscher, D.; Oldham, N. J.; Bartram, S.; Schneider, B. Phenylphenalenone-related compounds: Chemotaxonomic markers of the Haemodoraceae from *Xiphidium caeruleum*. *J. Nat. Prod.* **2002**, *65*, 1122-1130.
26. Flors, C.; Nonell, S. Light and singlet oxygen in plant defense against pathogens: Phototoxic phenalenone phytoalexins. *Acc. Chem. Res.* **2006**, *39*, 293-300.
27. Bucher, G.; Bresoli-Obach, R.; Brosa, C.; Flors, C.; Luis, J.G.; Grillo, T. A.; Nonell, S. β -Phenyl quenching of 9-phenylphenalenones: A novel photocyclisation reaction with biological implications. *Phys. Chem. Chem. Phys.* **2014**, *16*, 18813-18820.
28. Røeggen, I.; Johansen, T. Cholesky decomposition of the two-electron integral matrix in electronic structure calculations. *J. Chem. Phys.* **2008**, *128*, 194107.
29. Forsberg, N.; Malmqvist, P.-Å. Multiconfiguration perturbation theory with imaginary level shift. *Chem. Phys. Lett.* **1997**, *274*, 196-204.
30. Malmqvist, P.-Å.; Roos, B. O. The CASSCF state interaction method. *Chem. Phys. Lett.* **1989**, *155*, 189-194.
31. Aquilante, F.; De Vico, L.; Ferré, N.; Ghigo, G.; Malmqvist, P. A.; Neogrády, P.; Pedersen, T. B.; Pitonak, M.; Reiher, M.; Roos, B. O.; Serrano-Andrés, L.; Urban, M.; Veryazov, V.; Lindh, R. MOLCAS 7: the next generation. *J. Comput. Chem.*, **2010**, *31*, 224-247.
32. Frisch, M. J.; Trucks, G. W.; Schlegel, H. B.; Scuseria, G. E.; Robb, M. A.; Cheeseman, J. R.; Scalmani, G.; Barone, V.; Mennucci, B.; Petersson, G. A. et al. Gaussian, Inc.: Wallingford, CT, USA, 2009.

